IJMS
Vol 46, No 6, November 2021

Original Article

Engineering of Ocriplasmin Variants by Bioinformatics Methods for the Reduction of Proteolytic and Autolytic Activities

Roghayyeh Baghban[1,2,3], PhD; Safar Farajnia[4], PhD; Younes Ghasemi[5,6], PhD; Mojtaba Mortazavi[7], PhD; Samaneh Ghasemali[1], PhD; Mostafa Zakariazadeh[8], PhD; Nosratollah Zarghami[1], PhD; Nasser Samadi[1], PhD

[1]Department of Medical Biotechnology, School of Advanced Medical Science, Tabriz University of Medical Sciences,Tabriz, Iran;
[2]Student Research Committee, Tabriz University of Medical Sciences, Tabriz, Iran;
[3]Poostchi Ophthalmology Research Center, Shiraz University of Medical Sciences, Shiraz, Iran;
[4]Drug Applied Research Center, Tabriz University of Medical Sciences, Tabriz, Iran;
[5]Pharmaceutical Sciences Research Center, School of Pharmacy, Shiraz University of Medical Sciences, Shiraz, Iran;
[6]Department of Pharmaceutical Biotechnology, School of Pharmacy, Shiraz University of Medical Sciences, Shiraz, Iran;
[7]Department of Biotechnology, Institute of Science and High Technology and Environmental Sciences, Graduate University of Advanced Technology, Kerman, Iran;
[8]Department of Biology, Payame Noor University, Tehran, Iran

Correspondence:
Safar Farajnia, PhD;
Biotechnology Research Center, Tabriz University of Medical Sciences, Daneshgah Ave., Postal code: 51666-14776, Tabriz, Iran
Tel: +98 9143018589
Fax: +98 41 33363432
Email: farajnias@tbzmed.ac.ir
Received: 20 June 2020
Revised: 05 September 2020
Accepted: 06 September 2020

What's Known

- At physiological pH, ocriplasmin is very autolytic and proteolytic, which restricts its activity duration. Proteolytic activity can lead to photoreceptor damage and vision loss in more serious cases.
- Ocriplasmin suffers autolytic degradation after injection into the vitreous, resulting in its fast inactivation.

What's New

- Three ocriplasmin variants were designed via site-directed mutagenesis, and the mutational analysis of the variants was performed through homology modeling, molecular docking, and molecular dynamic simulations.
- Our *in silico* mutational analysis of ocriplasmin revealed that A59T and K156E mutagenesis could be used to develop new ocriplasmin variants with higher therapeutic efficacy.

Abstract

Background: Ocriplasmin has been developed for the induction of posterior vitreous detachment in patients with vitreomacular adhesion. At physiological pH, ocriplasmin is susceptible to autolytic and proteolytic degradation, limiting its activity duration. These undesirable properties of ocriplasmin can be reduced by site-directed mutagenesis, so that its enzymatic activities can be augmented. This study aimed to design ocriplasmin variants with improved biological/physicochemical characteristics via bioinformatics tools.

Methods: This study was performed in Tabriz University of Medical Sciences, Tabriz, Iran, 2019. Through site-directed mutagenesis, three ocriplasmin variants were designed. Structural analysis was performed on the wild-type variant and the mutant variants using the Protein Interactions Calculator (PIC) server. The interactions between the S-2403 substrate and the ocriplasmin variants were studied by molecular docking simulations, and binding capability was evaluated by the calculation of free binding energy. The conformational features of protein-substrate complex systems for all the variants were evaluated using molecular dynamic simulations at 100 nanoseconds.

Results: The structural analysis of ocriplasmin revealed that the substitution of threonine for alanine 59 significantly reduced proteolytic activity, while the substitution of glutamic acid for lysine 156 influenced autolytic function. The molecular docking simulation results indicated the appropriate binding of the substrate to the ocriplasmin variants with high-to-low affinities. The binding affinity of the wild-type variant for the substrate was higher than that between the mutant variants and the substrate. Simulation analyses, consisting of the root-mean-square deviation, the root-mean-square fluctuation, and the center-of-mass average distance showed a higher affinity of the substrate for the wild type than for the mutant variants.

Conclusion: The mutational analysis of ocriplasmin revealed that A59T and K156E mutagenesis could be used for the development of a new variant with higher therapeutic efficacy.

Please cite this article as: Baghban R, Farajnia S, Ghasemi Y, Mortazavi M, Ghasemali S, Zakariazadeh M, Zarghami N, Samadi N. Engineering of Ocriplasmin Variants by Bioinformatics Methods for the Reduction of Proteolytic and Autolytic Activities. Iran J Med Sci. 2021;46(6):454-467. doi: 10.30476/ijms.2020.86984.1705.

Keywords ● Mutagenesis ● Site-directed ● Molecular docking simulation ● Molecular dynamics simulation

Introduction

Ocriplasmin (formerly "microplasmin" and trade name "Jetrea")

is a novel FDA-approved pharmacological agent for the treatment of various vitreoretinopathies such as symptomatic vitreomacular adhesion and vitreomacular traction. Ocriplasmin, with a molecular weight of 27 kDa, is a recombinant truncated form of human plasmin with serine (Ser) protease activity.[1] Before the FDA approval of ocriplasmin, the only treatment for vitreomacular adhesion was the surgical method of vitrectomy.[2] This surgical modality carries the risk of retinal damage, which explains why some plasmin-containing proteolytic enzymes have been trialed for the enzymatic release of retinal traction.[3] While ocriplasmin might avert the risk of surgical treatment, pharmacologic vitreolysis is not devoid of risk.[4] The proteolytic and autolytic nature of this enzyme at physiological pH limits its activity duration. Proteolytic activity can lead to photoreceptor damage and even vision loss in more serious cases.[5, 6] Specific plasmin inhibitors such as α2-antiplasmin, α2-macroglobulin, and α2-antitrypsin can be found in the vitreous under normal and disease conditions, and they can influence its function.[6] It should, therefore, come as no surprise that the vitreous may sustain extensive damage from an enzyme with wide substrate specificity and high proteolytic activity.[3] Moreover, ocriplasmin suffers autolytic degradation after injection into the vitreous, which leads to its fast inactivation.[7]

Molecular dynamic (MD) simulations, as a computational predictive method, can be used successfully to analyze the motions of ions, water, macromolecules, and further complex systems. Specifically, structure/function relationships such as those that are reliant on the solute/solvent and temperature are essential to the determination of the paradigm of protein-protein or ligand-protein complexes. Indeed, the fact that these motions can be modeled by MD simulations attests to the utility of this predictive method.[8] Amino acid mutation analysis has rapidly evolved into dynamic research in the computational studies of proteins. This is mainly related not only to the availability of growing levels of protein sequences throughout the post-genomic era, which confers a rapid collection of data on protein variations, but also to many new bioinformatics tools for the investigation of the consequences and effects of amino acid mutation. Mutated proteins are crucial both to a more in-depth understanding of protein functions and genotype-phenotype relationships and to a more rational design and engineering of therapeutic proteins.[9] Computational mutagenesis revealed that some mutations may have an important role in diminishing the autolytic and proteolytic activities of ocriplasmin and producing an optimized enzyme. Previously, the structure of microplasmin (ocriplasmin), in conjunction with its active sites, proteolytic sites, and autolytic sites, has been determined.[7, 10] The key amino acids in the active site/proteolytic site of ocriplasmin comprise the catalytic triad of aspartic acid (Asp), histidine (His), and Ser, whose hydroxyl sidechain is responsible for nucleophilic attacks to the peptide substrate in the catalytic mechanism. In the active form of ocriplasmin, the catalytic triad of Ser-His-Asp (S199, H61, and D104 in ocriplasmin) forms a compact unit with the His sidechain that is centrally located and hydrogen-bonded to both Asp and Ser.[10]

The major autolytic cleavage sites are limited to three positions: K156–E157, K166–V167, and R177–V178. All of them align with the cleavage-site specificity of ocriplasmin, which is prone to cleavage after being positively charged with lysine (Lys) or arginine residues. The first cleavage occurs at position 156–157, as it is faster; and after this cleavage, the sensitivity of the other sites to cleavage is greatly enhanced.[7] Therefore, the substitution of glutamic acid (Glu) for Lys is more effective than that for other amino acids in the reduction of autolytic activity.[3] In dysplasminogenemia, the functional activity of plasminogen is diminished. The mutation of Ala601Thr has been described in dysplasminogenemia, and the substitution of threonine (Thr) for alanine 601 plays an important role in the reduction of the functional activity of plasminogen. (Alanine 601 in plasminogen is equivalent to alanine 59 [Ala59] in ocriplasmin).[11]

In this study, three variants of ocriplasmin, each containing one mutation, were designed. In the first variant, termed “the autolytic variant”, Lys156 was mutated to Glu to reduce autolytic activity. In the second variant, termed “the proteolytic variant”, Ala59 was mutated to Thr to lessen proteolytic activity. The third variant, termed “the mixed variant”, comprised both mutations (A59T and K156E). In addition, the wild-type variant lacked any mutation. For the bioinformatics analysis of the different features of ocriplasmin, the 3D structure of ocriplasmin was modeled by I-TASSER and Swiss Model webservers.[12, 13] Subsequently, the position of these mutations was studied by Swiss-PdbViewer and PyMOL software tools.[14, 15] Thereafter, molecular docking simulations were performed to study the interactions between the Chromogenix S-2403 substrate (L-pyroglutamyl-L-phenylalanyl-L-lysine-p-nitroaniline hydrochloride, Chromogenix, Milano, Italy, cat. 822254-39 as a chromogenic substrate for plasmin, ocriplasmin, and

streptokinase-activated plasminogen) and the ocriplasmin variants. Afterwards, the binding capability was evaluated by calculating free binding energy values. Finally, for the assessment of the conformational features of protein-substrate complex systems for the wild-type variant and all the mutant variants of ocriplasmin, MD simulations at 100 nanoseconds were performed.

Methods

Sequence Availability

This study was performed in Tabriz University of Medical Sciences, Tabriz, Iran, 2019. The amino acids and the accession number (DB08888 [DB05028]) of ocriplasmin were retrieved from the DrugBank database and saved in FASTA format for further analyses.

Three- and Two-dimensional Structure Prediction Using Homology Modeling

The 3D structure of the ocriplasmin was predicted via an automated homology modeling approach in the (PS)2v2 server (http://ps2.life.nctu.edu.tw/).[16] A combination of PSI-BLAST, IMPALA, and T-Coffee methods was used by the server to perform the necessary template selection and target-template alignment. In addition to the modeling procedure on this server, the 3D structure of the ocriplasmin enzyme was modeled in the I-TASSER and Swiss Model webservers.[12, 13] In the I-TASSER webserver, through the application of the crystal structure of similar enzymes, 3D models were built by LOMETS and iterative template fragment assembly simulations.[17] The I-TASSER webserver produced five models of ocriplasmin. Models with the best confidence score (C-score) and standard score (Z-score) were chosen, and the locations of these mutations were visualized and studied using the Swiss-PdbViewer and PyMOL software tools.[14, 15] The secondary structure of ocriplasmin was predicted in the SYMPRED webserver.[18] The secondary structure of this protein was also predicted in the PSIPRED and SOPMA webservers.[19, 20] Energy minimization was performed using the YASARA force field (http://www.yasara.org/minimizationserver.htm). For the mutant variants, the mutated amino acid was first changed in the linear sequence of amino acids. Then, this changed sequence was introduced to the I-TASSER webserver, and the structure of the mutant enzyme was modeled. Subsequently, other studies similar to that on the wild-type enzyme were performed on these mutant enzymes.

Physicochemical Properties of the Models

The physicochemical properties of the native and mutant proteins, comprising the molecular weight, the theoretical isoelectric point (pI), the amino acid composition, the whole number of negatively and positively charged residues, the instability index, and the aliphatic index, were determined. Additionally, hydrogen bonds were estimated using the WHAT IF and PIC webservers.[21, 22]

Molecular Docking Simulation Study

Models of all the variants of ocriplasmin with the S-2403 substrate were evaluated using molecular docking simulations to study the interaction manner of this substrate in the 3D structure of ocriplasmin and its binding capability by calculating free binding energy values. Therefore, the freely available packages of AutoDock 4.2.6 and AutoDock Tools 1.5.6 were used.[23] The 2D chemical structure of the S-2403 substrate was achieved using the ChemDraw Ultra 10.0 software,[24] and the molecular energy optimization of this structure was performed via molecular mechanics (MM+) and semi-empirical (AM1) approaches for the optimization of the structure. The Fletcher–Reeves algorithm was applied during the optimization procedure. The HyperChem 8.0.8 software was utilized for the aforementioned optimization procedure.[25]

The molecular structures of all the variants of ocriplasmin (wild, proteolytic, autolytic, and autolytic/proteolytic mutant types), which were used as macromolecules in the molecular docking simulation study, were prepared via the homology modeling knowledge-based protein tertiary structure prediction method. Molecular docking simulations were performed in the proteolytic site/active site (Ala59, His61, Asp104, and Ser199) and the autolytic site (Lys156 and Glu157) of all the ocriplasmin variants to assay their substrate-binding potency and to assess the efficacy of this binding in decreasing autolytic and proteolytic activities. In the first step, autolytic and proteolytic sites were defined for the molecular docking simulations of the substrate in all the variants independently. Then, according to the obtained results of docking in the first step, a high-number conformations cluster-binding site was selected for the focus docking approach in the second step. In this step, the size of the grid box dimensions at grid points in x×y×z directions was set to 62×62×62 $Å^3$ (0.375 Å grid spacing) for ocriplasmin in all the variants. The center of the grid box in x, y, z centers was fixed to -42.95, 31.70, and -12.78. During the preparation of the substrate and macromolecule structures for docking, polar

hydrogen, charges of the Gasteiger-type and Kollman were added using the AutoDock Tools software. The Lamarckian genetic algorithm approach with 100 runs of the genetic algorithm was performed in this molecular docking simulation study for the substrate-wild-type, substrate-proteolytic-type, substrate-autolytic-type, and substrate-autolytic/proteolytic-type ocriplasmin systems.[26]

Simulation Setup

Four different protein-substrate complex systems were provided. Then, MD simulations at 100 nanoseconds were performed for all the systems using the GROMACS 2016 package. All the simulations were directed with GROMOS96 54A7 via the simple-point-charge water model.[27] The topology and parameter files of the designed substrates were prepared with the PRODRG webserver.[28] The solvated systems in explicit water molecules extended 10 A° from each edge of the cubic box to the solute atoms.[29] These systems were energy-minimized via the steepest descent approach and equilibrated under constant pressure (NPT) and volume (NVT) ensemble conditions, for 200 ps. For the visualization of the simulation results, the UCSF Chimera and VMD 1.9 software tools were utilized.[30, 31] With the aid of the UCSF Chimera package, total molecular graphics were produced.[30] Trajectory snapshots were saved every two fs through the simulation time, and 3D coordinate files were collected every two nanoseconds for post-dynamic evaluation. With the use of NaCl counterions, the systems were neutralized. After the addition of a proper number of the ions of sodium (Na^+) and chloride (Cl^-), the NaCl concentration in all the systems was 100 mM. Short-range non-bonded interactions, in all the systems, were truncated at 1.2 nm through a long-range correction to pressure and energy terms to account for the truncated Van der Waals forces. Additionally, the particle-mesh Ewald (PME) approach was applied for the calculation of the electrostatic energy of the interactions. Moreover, the LINear Constraint Solver (LINCS) algorithm was utilized for all the constraints, providing an integration time-step of 2 fs.[32] In all the directions, periodic boundary conditions were used. The temperature of the system was conserved at 300 °K with the Berendsen weak-coupling approach, and the pressure was preserved at 1 bar through the application of the Parrinello–Rahman barostat in the constant-pressure ensemble.[33] Additionally, the root mean square deviation (RMSD), the root-mean-square fluctuation (RMSF), Dictionary of Secondary Structure for Proteins (DSSP), and hydrogen bonds were analyzed throughout the MD simulation.

Comparison of the Center-of-Mass Distance between Ocriplasmin and the Substrate

For the investigation of the affinity between ocriplasmin and the substrate, the center-of-mass distance between the ocriplasmin active site and the substrate during the MD simulation was calculated. His61, Asp104, and Ser199 in the active site residues had an outstanding role in the interaction between the substrate and the ocriplasmin variants. The center-of-mass distance between the ocriplasmin active site and the substrate in the wild-type variant and all the mutant variants (A59T, K156E, and the mixed form) was also calculated during the simulation. Finally, the center-of-mass distance was compared between the active site residues and the substrate in all the variants.

Results

Sequence Availability and Amino Acid Composition

The amino acid sequence of ocriplasmin, containing 249 amino acids, was stored in a FASTA file format, and its feature was deposited in table 1.

Secondary Structure

The secondary structure components in ocriplasmin encompassed α-helix 15.26%, extended strand 29.72%, β- turn 0.00%, and random coil 55.02%. The situation of each amino acid in the secondary structure of ocriplasmin, and its plot showed that this sequence had one helix-turn-helix (HTH) motif, which is a DNA-binding motif.

Three-dimensional Structure Prediction and Physicochemical Properties of the Models

For the investigation of the 3D structure of ocriplasmin, the I-TASSER webserver was employed. The server produced five models. The best model displayed a total C-score of 1.60, a template modeling score (TM-score) of 0.94±0.05, and an estimated RMSD of 3.4±2.4. Table 2 illustrates the physicochemical features of the ocriplasmin model, which were estimated using the ProtParam software. Thereafter, the structural models of ocriplasmin were precisely studied for the location of the A59T and K156E mutations. The results showed that these mutations were distributed in different regions of the ocriplasmin structure. The 3D structure of ocriplasmin, which was modeled in the I-TASSER

Table 1: The features of the amino acid sequence of ocriplasmin

Residues	Number	Percentage	Residue Mass	Specific Volume
Ala	14	5.62	90.10	0.74
Asx	0	0.00	133.61	0.61
Cys	12	4.82	122.16	0.63
Asp	7	2.81	134.11	0.60
Glu	16	6.43	148.13	0.66
Phe	9	3.61	166.20	0.77
Gly	25	10.04	76.07	0.64
His	7	2.8	156.16	0.67
Ile	10	4.02	132.18	0.90
Lys	13	5.22	147.19	0.82
Leu	21	8.43	132.18	0.90
Met	2	0.8	150.22	0.75
Asn	8	3.21	133.12	0.62
Pro	19	7.63	116.13	0.76
Gln	9	3.61	147.15	0.67
Arg	13	5.22	175.21	0.70
Ser	16	6.43	106.10	0.63
Thr	13	5.22	120.12	0.70
Val	24	9.64	118.15	0.86
Trp	6	2.41	205.23	0.74
Unk	0	0.00	138.15	0.72
Tyr	5	2.01	182.19	0.71
Glx	0	0.00	147.64	0.67
Total	249	100.00	27232.47 Da	

Table 2: The *in silico* physicochemical features of ocriplasmin achieved from the ProtParam webserver

No.	Parameters	Wild Type	A59T	K156E	A59T and K156E
1	Theoretical pI	8.27	8.27	7.67	7.67
2	Molecular weight	27231.34	27261.36	27232.28	27262.31
3	Sequence length	249	249	249	249
4	Extinction coefficient	41200-40450	41200-40450	41200-40450	41200-40450
5	Asp+Glu	23	23	24	24
6	Arg+Lys	26	26	25	25
7	Instability index	48.35	48.35	50.00	50.00
8	Grand average of hydropathicity	-0.14	-0.15	-0.14	-0.15
9	Aliphatic index	82.13	81.73	82.13	81.73

* The first value is according to the hypothesis that both cysteine residues are oxides and form cystine, and the second value is based on the hypothesis that supposes, which of the cysteine residues is decreased. pI: Isoelectric point

Table 3: The calculation and characteristics of the hydrogen bonds between Ala59 and the other residues

Donors			Acceptors			Parameters			
POS	RES	ATOM	POS	RES	ATOM	Dd-a	Dh-a	A(d-HN)	A(aO=)
61	His	N	59	Ala	O	3.27	3.38	75.07	77.57
62	Cys	N	59	Ala	O	3.02	2.18	141.76	126.25
62	Cys	N	59	Ala	O	3.02	2.18	141.76	126.25
62	Cys	N	59	Ala	O	3.02	2.18	141.76	126.25

POS: Position; RES: Residue; Dd-a: Distance between donor and acceptor; Dh-a: Distance between hydrogen and acceptor; A(d-H-N): Angle between donor-H and donor-N; A(a-O=C): Angle between acceptor-O and acceptor-C

webserver, along with A59 and K156, is depicted in figure 1A. Subsequently, the location of A59 and K156 was precisely evaluated in this model. The analysis of this 3D model showed that the Ala59 residue formed a hydrogen bond with His61 and Cys62 (figure 1B[a]). However, not all of these hydrogen bonds could be shown in the structure viewer software, which is a limitation defined for this software. The computation of non-covalent interactions was performed with the WHAT IF and PIC webservers. The results of these evaluations are presented in table 3. The substitution of Thr for Ala59 had a significant role in the reduction of the proteolytic activity of the enzyme. The mutation of

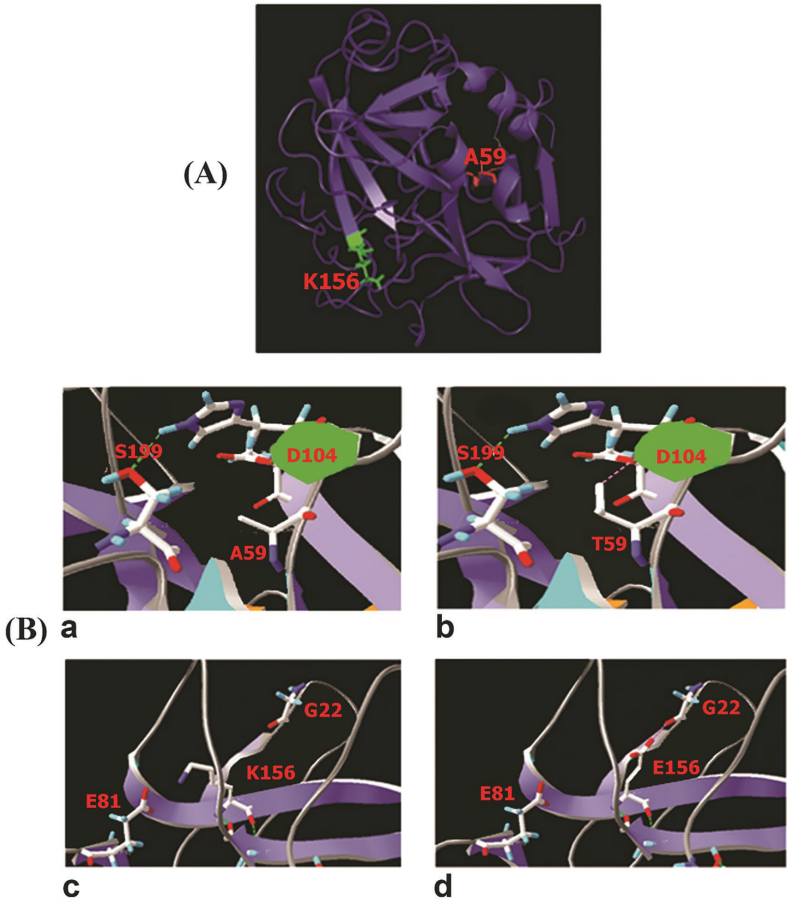

Figure 1: The images illustrate the 3D structure of ocriplasmin modeled in the I-TASSER webserver. (A) The figure shows the location of A59 and K156, (B) (a) the non-covalent interactions between Ala59 and the other residues (D104 and S199), (b) the non-covalent interactions between Thr59 and the other residues (D104 and S199), (c) the non-covalent interactions between K156 and the other residues (G22 and E81), and (d) the non-covalent interactions between Glu156 and the other residues (G22 and E81).

Table 4: The calculation and characteristics of the hydrogen bonds between K156 and the other residues

Donors				Acceptors				Parameters			
POS	ATOM	RES	ATOM	POS	ATOM	RES	ATOM	Dd-a	Dh-a	A(d- HN)	A(aO=C)
142	A	Gly	N	156	A	Lys	O	2.99	2.04	159.55	160.07
156	A	Lys	N	142	A	Gly	O	2.96	2.12	138.80	143.98
156	A	Lys	NZ	143	A	Trp	O	2.69	9.99	999.99	126.11
156	A	Lys	NZ	154	A	Leu	O	2.74	9.99	999.99	142.28
156	A	Lys	NZ	81	A	Glu	OE1	2.95	9.99	999.99	999.99
156	A	Lys	NZ	81	A	Glu	OE2	2.99	9.99	999.99	999.99

POS: Position; RES: Residue; Dd-a: Distance between donor and acceptor; Dh-a: Distance between hydrogen and acceptor; A(d-H-N): Angle between donor-H and donor-N; A(a-O=C): Angle between acceptor-O and acceptor-C

Ala59 to Thr59 was followed by a change in some non-covalent interactions and the creation of new interactions (figure 1B[b]).

Evaluation of the 3D model of ocriplasmin showed that the K156 residue constituted hydrogen bonds (figure 1B [c]). The results of this study are presented in table 4. The results also demonstrated that the substitution of Glu for Lys156 significantly influenced autolytic function. The mutation of Lys156 to Glu156 was followed by a change in some non-covalent interactions and the creation of new interactions (figure 1B[d]).

Molecular Docking Simulation Study

The chemical and optimized structures of the S-2403 substrate are illustrated in figure 2A and figure 2B, respectively. This substrate was used for docking simulations with the enzyme variants of ocriplasmin. The results obtained from the molecular docking simulation studies of the S-2403 substrate with the different variants of the ocriplasmin enzyme indicated that the lowest free binding energy values (ΔG) between them in the high-number conformations cluster were -7.67, -6.93, -6.75, and -5.84 kcal mol^{-1} for the substrate-wild-type,

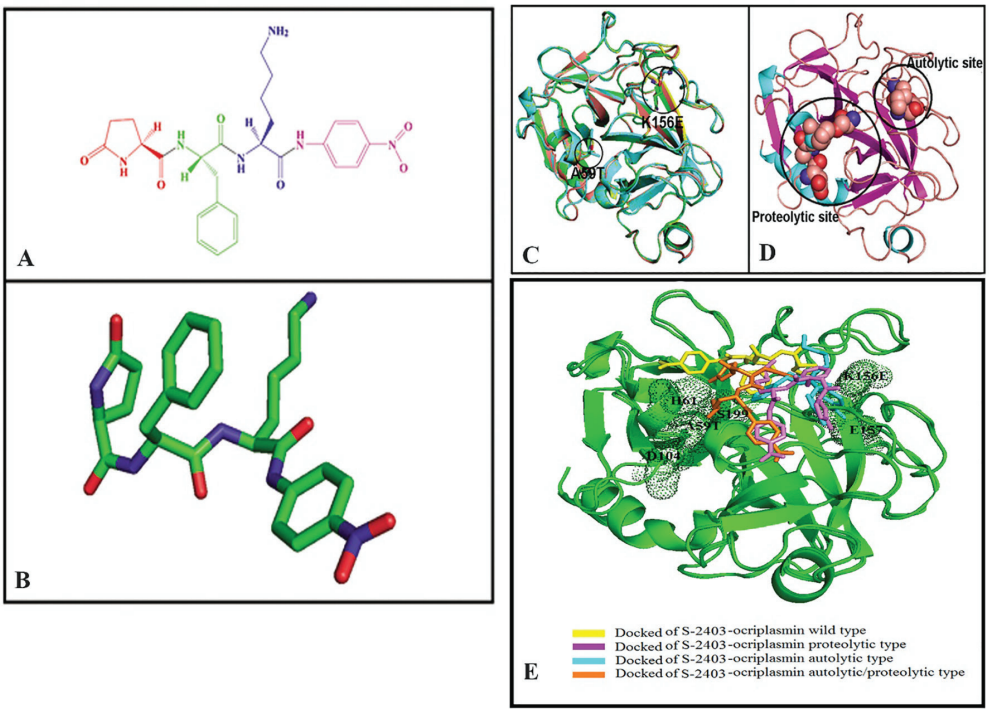

Figure 2: The images illustrate the structures of the substrate and the ocriplasmin variants and the substrate docked to the four variants of ocriplasmin. The figure presents (A) the chemical structure of the substrate, (B) the optimized 3D structure of the substrate, and (C) the superimposed structures of the wild and mutant types of ocriplasmin. Ala, Thr, Lys, and Glu residues are indicated with sticks. (D) The image depicts the proteolytic and autolytic sites of ocriplasmin. Important residues are indicated with spheres. (E) The image presents the docking simulation results of the interactions between the substrate and the four variants of ocriplasmin.

substrate-autolytic-type, substrate-proteolytic-type, and substrate-autolytic/proteolytic-type ocriplasmin systems, respectively. Nonetheless, the mean free binding energy values (ΔG_{mean}) for the associated clusters were -6.80, -6.03, -5.84, and -5.21 kcal mol^{-1}, correspondingly. Figure 2C presents the wild-type variant and the three mutant variants of ocriplasmin aligned, figure 2D shows the proteolytic and autolytic sites, and figure 2E demonstrates the docked substrate with all the variants of ocriplasmin. These results of the molecular docking simulations indicated that whereas there was a high affinity between the substrate and the wild-type ocriplasmin variant, the affinity of the substrate for the mutant autolytic/proteolytic variant of ocriplasmin was low. In addition, the interaction potency was stronger between the substrate and the autolytic mutant variant than between the substrate and the proteolytic mutant variant. The *in silico* molecular docking simulation results showed that the mutation of Ala59 to Thr, by comparison with the mutation of Lys156 to Glu, in the proteolytic site exerted a marked effect on the binding capability of the substrate to ocriplasmin. Nevertheless, both mutations had a pronounced effect on the binding potency of the substrate to the autolytic/proteolytic mutant variant. To better understand the effect of the mutation of Ala59 to Thr on the proteolytic activity of ocriplasmin, we pointed to the catalytic triad residues (Asp104, His61, and Ser199) in the active site. These catalytic triads constitute the major residues of Ser proteases that participate in the catalytic mechanism. In the 3D structure of ocriplasmin, Ala59 was positioned between Asp104 and His61. In the wild and autolytic ocriplasmin variants, where Ala59 was not mutated, the distance between the oxygen atom of the carboxylic acid group in Asp104 and the nitrogen atom of the imidazole ring of His61 was 2.8 Å and 2.9 Å, respectively. These distances are appropriate for the formation of intramolecular hydrogen bonds. By contrast, the mutation of Ala59 to Thr in the proteolytic and autolytic/proteolytic ocriplasmin variants significantly influenced the distance between these residues, where the distance between Asp104 and His61 changed to 5.9 Å and 4.5 Å, respectively. Therefore, these ocriplasmin variants failed to form a hydrogen bond between Asp104 and His61, and Thr increased the distance between these essential amino acids. On the other hand, the high affinity of the S-2403 substrate for the wild and autolytic variants of ocriplasmin could be due to the formation of a hydrogen bond between Asp104 and His61, promoting the protease activity and stability of the active site. Notably, the distance between His61 and Ser199 underwent no

significant change in all the ocriplasmin variants, nor did they exert a direct effect on the catalytic mechanism. The conformers obtained from the docking of the substrate to the variants of ocriplasmin were analyzed separately to examine the formation of the most important non-covalent interaction, hydrogen bonding. All 100 runs, which were introduced at the beginning of docking for each system, were surveyed to find the hydrogen bonds formed between the residues and the functional groups of the peptide. According to the findings, the S-2403 substrate formed hydrogen bonds with His44, Phe45, Cys46, His61, Cys62, Glu64, Lys65, Glu81, Trp143, Gly144, Glu145, hr146, Asp193, Cys195, Gly197, Asp198, Ser199, Trp219, Gly220, Gly222, Cys223, and Arg225 in the substrate-wild-type ocriplasmin docking system. In the substrate-proteolytic-type ocriplasmin docking system, the amino acids participating in the formation of hydrogen bonds were Phe45, Cys46, His61, Glu64, Lys65, Gly144, Glu145, Asp193, Ser194, Cys195, Trp219, Gly220, Gly222, Cys223, and Arg225. In the substrate-autolytic-type ocriplasmin docking system, the residues were His44, Phe45, Cys46, His61, Cys62, Glu64, Lys65, Trp143, Gly144, Glu145, Thr146, Gln147, Glu157, Thr192, Asp193, Ser194, Cys195, Gly197, Asp198, Ser199, Ser218, Gly220, Cys223, and Arg225. Furthermore, Phe45, Cys46, His61, Glu64, Lys65, Gly144, Glu145, Cys195, Asp198, Ser199, Ser218, Trp219, Gly220, Gly222, Cys223, and Arg225 participated in the formation of hydrogen bonds with the autolytic/proteolytic type ocriplasmin mutant variant. Moreover, the most important amino acids that formed hydrogen bonds in all four ocriplasmin variants with the substrate were Phe45, Cys46, His61, Glu64, Lys65, Gly144, Glu145, Cys195, Ser199, Gly220, Cys223, and Arg225. In addition, His61 and Ser199 in the active site residues played an outstanding role in the interactions between the substrate and the ocriplasmin variants. Most of these residues belonged to the polar group amino acids, which formed hydrogen bonds with the amino and carbonyl functional groups of the substrate. Figure 3(A-D) illustrates a 3D presentation of the amino acids that interacted and formed hydrogen bonds with all the ocriplasmin variants in this molecular docking simulation study. The molecular docking simulation results indicated that the substrate possessed the appropriate ability to bind to the ocriplasmin variants with high-to-low affinities in the substrate-wild-type, substrate-autolytic-type, substrate-proteolytic-type, and substrate-autolytic/proteolytic-type ocriplasmin systems, respectively.

Conformational Dynamic Stability

The conformational features of the protein-substrate complex systems were evaluated through RMSD and RMSF assays. The RMSD values for the structures of the wild-type variant and the mutant variants of ocriplasmin were estimated against the simulation time to be between 0 and 100 nanoseconds. Figure 4A shows the backbone RMSD of the proteins in the simulated systems. As is depicted in figure 4A, all the systems were equilibrated through the simulation time and were analyzed at the atomic scale. All the mutant variants of ocriplasmin in complex with the S-2403 substrate had an RMSD change comparable with that of the wild-type

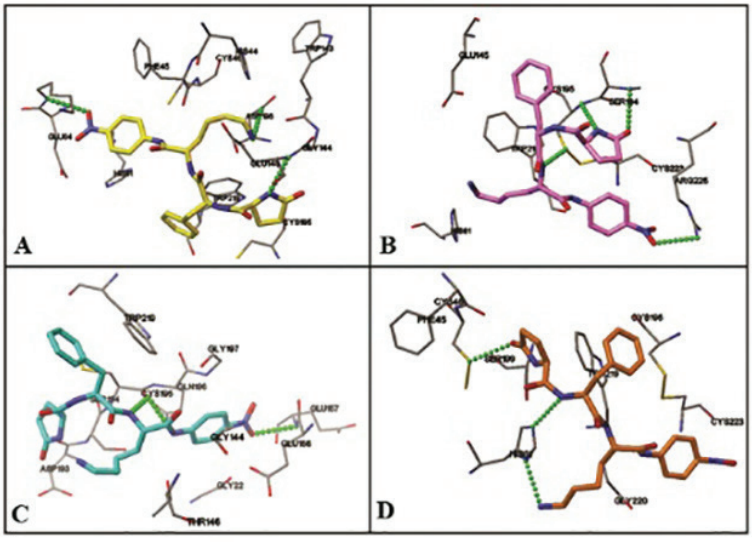

Figure 3: The images constitute a 3D representation of the interactions between the substrate and the ocriplasmin amino acids in the docked systems. The formed hydrogen bonds are depicted with green spheres. The figure shows (A) the substrate-wild-type, (B) substrate-proteolytic-type, (C) substrate-autolytic-type, and (D) substrate-autolytic/proteolytic-type ocriplasmin systems.

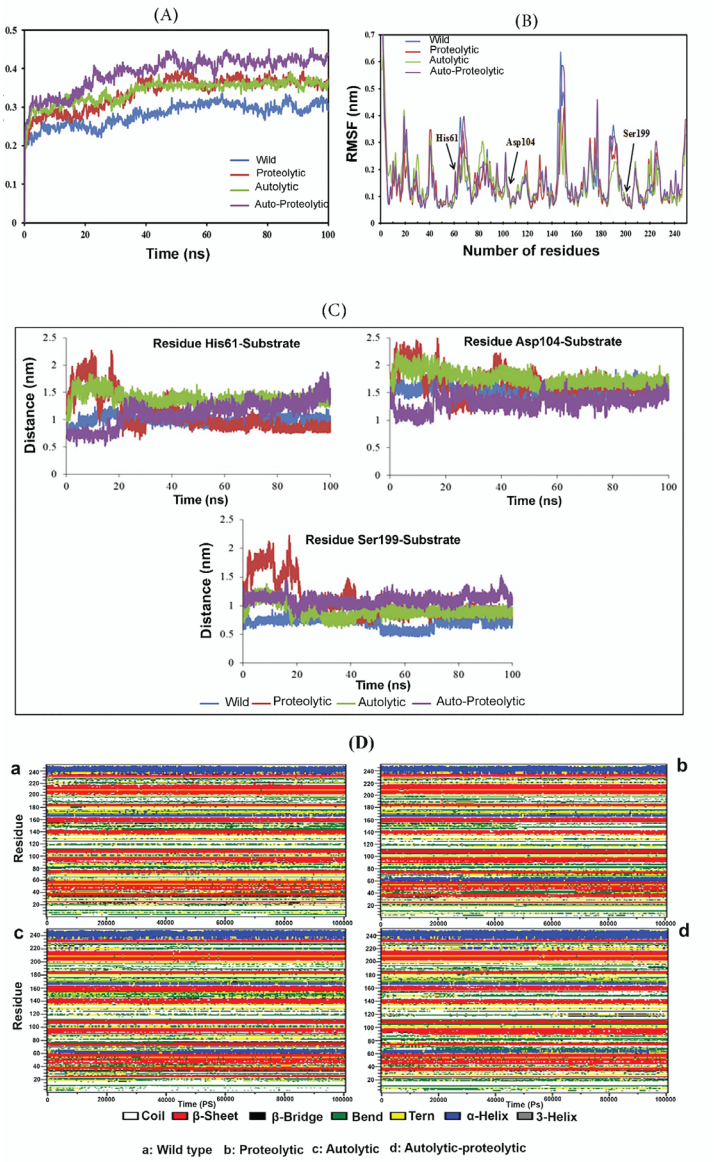

Figure 4: The images present computational simulation analyses, comprising RMSD, RMSF, the center-of-mass distance between the ocriplasmin variants and the substrate, and DSSP, throughout the MD simulation. (A) The RMSD of the backbone C-alpha atoms is shown as a function of time for all the ocriplasmin variants. (B) The RMSF of the backbone C-alpha atoms is shown as opposed to the residue numbers of all the ocriplasmin variants. (C) The image presents a comparison of the center-of-mass distance between the ocriplasmin variants and the substrate. (D) The image shows the secondary structural changes of all the ocriplasmin variants in complex with the substrate during the MD simulations. RMSD: Root mean square deviation; RMSF: Root-mean-square fluctuation; DSSP: Dictionary of Secondary Structure for Proteins; MD: Molecular dynamics

system. The average RMSD values for the three mutant variants of ocriplasmin in complex with the substrate (substrate-proteolytic, substrate-autolytic, and substrate-autolytic/proteolytic) were 0.33, 0.34, and 0.39 nm, respectively, and the substrate-wild-type ocriplasmin variant showed an average RMSD value of 0.28 nm throughout the simulation. The mutant systems were unstable with high structural changes in comparison with the wild-type state. Overall, all the mutant ocriplasmin systems in complex with the substrate, by comparison with the wild-type system, exhibited high structural changes, demonstrating the steady binding of the S-2403 substrate to the wild-type variant throughout the MD simulation as well as its high affinity for the wild-type variant.

For the determination of the conformational flexibility and dynamical behavior of each residue over the equilibrated simulation trajectories, RMSF values were calculated for the wild-type variant and the mutant ocriplasmin structures (figure 4B). The RMSF values during the MD simulation verified the RMSD data, and the mutant ocriplasmin-substrate systems showed higher fluctuations than the wild-type system. As was expected, N- and C-terminal residues represented high RMSF values in all

the simulated systems because of their high fluctuations. The RMSF values of the active site-located residues (His61, Asp104, and Ser199) in the wild-type variant were 0.10, 0.09, and 0.096, correspondingly. In the proteolytic variant, the RMSF values were 0.16, 0.11, and 0.20, respectively. Furthermore, the respective RMSF values in the autolytic and auto-proteolytic variants were 0.12, 0.10, and 0.11 and 0.19, 0.13, and 0.097. As a result, the RMSF value of the mutant structure of the ocriplasmin-substrate complex systems was greater than that of the wild-type system. Larger RMSF scales indicated the greater flexibility of the residues during the MD simulation. The applied substrate (S-2403) resulted in the enhanced rigidity of some residues and induced further fluctuations in the others. This implied that the interactions of the functional groups of substrates with some residues led to the increased rigidity of the backbone of the enzyme and the fluctuation of some non-interacting groups. Overall, the RMSF values for the active site-located residues (His61, Asp104, and Ser199) in the wild protein structure were relatively stable compared with the RMSF values for mutant types, which was mainly because of further interactions between the substrate and the wild-type ocriplasmin variant.

Comparison of the Center-of-Mass Distance between Ocriplasmin and the Substrate

The analysis of the center-of-mass distance between the mutant variants and the substrate, presented in figure 4C, demonstrated that the mutation of Ala59 to Thr (A59T) and Lys156 to Glu (K156E) increased the distance between the center-of-mass active site residues and the substrate. In the wild-type variant, by comparison with the mutant types, this distance was reduced during the simulation. Hence, these results indicated a decreased affinity in the mutant types in comparison with the wild-type variant.

Secondary Structure Analysis

The analysis of the secondary structure contents is a critical element to the evaluation of the structural manners of proteins during the simulation. The present study explored changes in the secondary structure contents of the wild-type variant and the three mutant variants of ocriplasmin (figure 4D). The percentages of the secondary structure contents in the wild-type variant and the mutant variants of ocriplasmin were approximately the same, and the differences were insignificant. These mutations did not induce any significant change in the contents of the secondary structure. However, as figure 4D clearly shows, the α-helix content in the mutant variant systems exhibited relatively significant increases compared with the wild-type variant. Moreover, by comparison with the wild-type variant, the bend content in the mutant variants exhibited a reduction. Nevertheless, the contents of β-bridge, β-sheet, random coil, 3_{10}-helix, and turn showed no significant changes among all the variants.

Hydrogen Bonds for the Wild Type and the Mutant Variants of the Ocriplasmin Structure

Hydrogen bonds play a critical role in the overall stability of the protein secondary structure and various molecular recognition events. In the current study, intermolecular hydrogen bonds were studied for the wild-type variant and the mutant structures of the ocriplasmin protein throughout the simulation time. Unsurprisingly, concerning hydrogen bonding, no significant differences were observed in ocriplasmin-substrate interactions between the wild-type variant and the mutant structures. The ligand used for all the enzyme variants was the same, and the mutated amino acids (A59T and K156E) in all the mutant ocriplasmin variants did not participate in the formation of any hydrogen bonds. Therefore, we expected no difference in the number of hydrogen bonds between the mutant variants.

Discussion

The findings of the present study indicated the appropriate ability of the substrate to bind to the variants of ocriplasmin with high-to-low affinities in the substrate-wild-type, substrate-autolytic-type, substrate-proteolytic-type, and substrate-autolytic/proteolytic-type ocriplasmin systems, respectively. The conformational features of protein-substrate complex systems for the wild-type variant and the mutant variants of ocriplasmin were evaluated via MD simulations at 100 nanoseconds. Generally, the results verified high structural changes in the mutant variants of ocriplasmin in complex with the substrate by comparison with the wild-type system. This demonstrated the steady binding of the S-2403 substrate to the wild-type variant throughout the MD simulation. Previous investigations revealed that MD simulations are reliable in modeling the wild- and mutant-state dynamics and their correlation with protein function.[34] Indeed, the high precision of MD simulations in terms of prediction has been proven previously.[35] Despite the feasibility of the experimental measurement of such landscapes, the capability to predict them computationally would both decrease the effort needed to collect the required data and offer an

advanced insight into critical interactions.[36] Our computational simulation analyses, comprising RMSD, RMSF, and the center-of-mass average distance, showed a higher affinity of the S-2403 substrate for the wild-type variant than for the mutant variants throughout the MD simulation. The RMSD and RMSF results revealed the stability and equilibration of the systems of all the variants over the simulation time and showed more fluctuations in the mutant variants of ocriplasmin in complex with the substrate. Overall, the RMSF values were greater for the mutant structures of ocriplasmin than for the wild type and showed increased flexibility around the active site-located residues (His61, Asp104, and Ser199). The RMSF values during the MD simulation verified the RMSD data, and the mutant ocriplasmin-substrate systems showed higher fluctuations than the wild-type system. Our analysis of the center-of-mass distance between the mutant variants and the substrate confirmed that the A59T and K156E mutagenesis increased the center-of-mass distance between the active site residues and the substrate. This distance was reduced in the wild type by comparison with the mutant variants during the simulation. Accordingly, these results indicated a diminished affinity in the mutant types compared with the wild type.

To our knowledge, we are the first to accomplish molecular docking simulation studies of the S-2403 substrate with ocriplasmin variants and MD simulations on the mutant variants of ocriplasmin (A59T and K156E) for an assessment of the structural effect of these mutations. Our results demonstrated that residues outside of the active site catalytic triad could change enzyme activity and stability. According to our calculated free binding energy (ΔG) values from the molecular docking simulation study, the S-2403 substrate had a higher affinity for the wild-type ocriplasmin variant and a lesser affinity for the autolytic/proteolytic ocriplasmin variant. Moreover, the affinity of this substrate for the autolytic and proteolytic variants was almost similar. The value of ΔG can be calculated by the sum of intermolecular energies (van der Waals+hydrogen bond+dissolving+electrostatic energies) minus the torsional free energy of the substrate by AutoDock software. The calculated intermolecular energies for the substrate-wild-type, substrate-autolytic-type, substrate-proteolytic-type, and substrate-autolytic/proteolytic-type ocriplasmin systems were -11.55, -10.81, -10.63, and -9.72 kcal mol^{-1}, respectively, and the substrate torsional free energy value was +3.88 kcal mol^{-1}. Regarding the molecular docking simulation results, although we described the formation of hydrogen bonds between the substrate and the ocriplasmin variant residues, it should be noted that hydrogen bonds and their frequencies are not the only significant parameters in the determination of the free binding energy value in the various substrate-ocriplasmin variants. In actuality, the absolute value of ΔG for any system is defined by different energies such as van der Waals, electrostatics, and the dissolution of hydrogen bonds. Our results in this respect are in agreement with other studies.[37] The substitution of Thr for Ala59 weakened the proteolytic activity of the enzyme, which is concordant with the finding reported by Song and colleagues.[11] Previous studies revealed that the autolytic inactivation of ocriplasmin occurs in the porcine vitreous at therapeutically-relevant concentrations. Autolytic cleavage takes place at several sites. All these cleavage sites are in agreement with the expected specificity of ocriplasmin, which is prone to cleavage after being positively charged with arginine or Lys residues. The most important autolytic cleavage site in ocriplasmin is 156–157, and this position greatly increases the susceptibility of the other sites to autolytic cleavage.[7] Moreover, the substitution of Glu for Lys, in comparison with other amino acids, exerts a significant effect on the reduction of autolytic activity.[3] Consequently, in the present study, of the three autolytic cleavage sites in ocriplasmin (K156–E157, K166–V167, and R177–V178), we opted for the substitution of Glu for Lys156 and witnessed a decrease in the autolytic activity of ocriplasmin.[12] These mutations appear to play a significant role in increasing the dynamical and structural flexibility of the catalytic core of the mutant variants. Our secondary structure analysis showed that the wild-type variant and the mutant variants of ocriplasmin shared almost similar secondary structure contents, with the differences between the variants being insignificant. According to our results, these mutations did not induce any significant changes in the secondary structure contents, nor was a difference expected regarding the number of hydrogen bonds between the different variants. We detected no significant differences in ocriplasmin-substrate interactions between the wild-type variant and the mutant structures of ocriplasmin. This finding can be explained by the fact that we used the same ligand for all the variants of the enzyme and that the mutated amino acids did not form any hydrogen bonds in all the mutant variants.

The efficacy of current *in silico* cell models is limited by our insubstantial understanding of cell biology, inadequate MD simulations, and insufficient computer processing powers.[38] The

drawbacks of *in silico* pharmacology approaches such as molecule conformation, protein flexibility, and protein promiscuity all impede precise predictions. For instance, despite the recent accessibility of crystal structures for numerous mammalian drug-metabolizing enzymes, metabolism predictions are still far from valid.[39] Be that as it may, the advantages of *in silico* methodologies cannot be ignored. The main advantage of these methods is their ability to fast-track the production rate and drug-candidate screening based on the study of evaluated properties and prediction models for drug targets, while they diminish the need for time-consuming and expensive *in vitro* and *in vivo* laboratory assays.[40]

Conclusion

We herein described different variants of ocriplasmin with enhanced resistance to autolytic and proteolytic activities. Our molecular docking simulation results indicated the appropriate ability of the substrate to bind to the variants of ocriplasmin with high-to-low affinities. Our computational simulation analyses, comprising RMSD, RMSF, and the center-of-mass average distance, showed a higher affinity of the S-2403 substrate for the wild-type variant than for the mutant variants throughout the MD simulation. The predicted 3D structure of ocriplasmin and their mutated variants can facilitate further structural, functional, and therapeutic research.

Acknowledgment

The authors herewith thank the Biotechnology Development Council and the Biotechnology Research Center, Tabriz University of Medical Sciences, for their support in the accomplishment of this work. This manuscript was extracted from the thesis by Roghayyeh Baghban. The study was financially supported by Tabriz University of Medical Sciences, Tabriz, Iran (grant number: 57829).

Conflict of Interest

Dr. Younes Ghasemi, Editor-in-Chief, was not involved in the peer-review and decision-making processes for this manuscript. The non-author Co-EIC oversaw the peer review process for this paper.

References

1 Khan MA, Haller JA. Ocriplasmin for Treatment of Vitreomacular Traction: An Update. Ophthalmol Ther. 2016;5:147-59. doi: 10.1007/s40123-016-0062-6. PubMed PMID: 27619226; PubMed Central PMCID: PMCPMC5125123.

2 Chin EK, Almeida DR, Sohn EH, Boldt HC, Mahajan VB, Gehrs KM, et al. Incomplete vitreomacular traction release using intravitreal ocriplasmin. Case Rep Ophthalmol. 2014;5:455-62. doi: 10.1159/000370024. PubMed PMID: 25606039; PubMed Central PMCID: PMCPMC4296250.

3 Noppen B, Fonteyn L, Aerts F, De Vriese A, De Maeyer M, Le Floch F, et al. Autolytic degradation of ocriplasmin: a complex mechanism unraveled by mutational analysis. Protein Eng Des Sel. 2014;27:215-23. doi: 10.1093/protein/gzu015. PubMed PMID: 24795342.

4 Silva RA, Moshfeghi DM, Leng T. Retinal breaks due to intravitreal ocriplasmin. Clin Ophthalmol. 2014;8:1591-4. doi: 10.2147/OPTH.S68037. PubMed PMID: 25210426; PubMed Central PMCID: PMCPMC4154885.

5 Beebe DC. Understanding the adverse effects of ocriplasmin. JAMA Ophthalmol. 2015;133:229. doi: 10.1001/jamaophthalmol.2014.4484. PubMed PMID: 25376025.

6 de Smet MD, Jonckx B, Vanhove M, van Calster J, Stalmans P, Stassen JM. Pharmacokinetics of ocriplasmin in vitreous. Invest Ophthalmol Vis Sci. 2012;53:8208-13. doi: 10.1167/iovs.12-10148. PubMed PMID: 23150619.

7 Aerts F, Noppen B, Fonteyn L, Derua R, Waelkens E, de Smet MD, et al. Mechanism of inactivation of ocriplasmin in porcine vitreous. Biophys Chem. 2012;165-166:30-8. doi: 10.1016/j.bpc.2012.03.002. PubMed PMID: 22445213.

8 Hernandez-Rodriguez M, Rosales-Hernandez MC, Mendieta-Wejebe JE, Martinez-Archundia M, Basurto JC. Current Tools and Methods in Molecular Dynamics (MD) Simulations for Drug Design. Curr Med Chem. 2016;23:3909-24. doi: 10.2174/0929867323666160530144742. PubMed PMID: 27237821.

9 Chen J, Shen B. Computational analysis of amino acid mutation: a proteome wide perspective. Current Proteomics. 2009;6:228-34. doi: 10.2174/157016409789973734.

10 Millers EK, Johnson LA, Birrell GW, Masci PP, Lavin MF, de Jersey J, et al. The structure of human microplasmin in complex with textilinin-1, an aprotinin-like inhibitor from the Australian brown snake. PLoS One. 2013;8:e54104. doi: 10.1371/journal.pone.0054104. PubMed PMID: 23335990;

PubMed Central PMCID: PMCPMC3545990.
11 Song KS, Lee SM, Choi JR. Detection of an Ala601Thr mutation of plasminogen gene in 3 out of 36 Korean patients with deep vein thrombosis. J Korean Med Sci. 2003;18:167-70. doi: 10.3346/jkms.2003.18.2.167. PubMed PMID: 12692411; PubMed Central PMCID: PMCPMC3055032.
12 Yang J, Zhang Y. Protein Structure and Function Prediction Using I-TASSER. Curr Protoc Bioinformatics. 2015;52:5 8 1-5 8 15. doi: 10.1002/0471250953.bi0508s52. PubMed PMID: 26678386; PubMed Central PMCID: PMCPMC4871818.
13 Biasini M, Bienert S, Waterhouse A, Arnold K, Studer G, Schmidt T, et al. SWISS-MODEL: modelling protein tertiary and quaternary structure using evolutionary information. Nucleic Acids Res. 2014;42:W252-8. doi: 10.1093/nar/gku340. PubMed PMID: 24782522; PubMed Central PMCID: PMCPMC4086089.
14 Kaplan W, Littlejohn TG. Swiss-PDB Viewer (Deep View). Brief Bioinform. 2001;2:195-7. doi: 10.1093/bib/2.2.195. PubMed PMID: 11465736.
15 DeLano WL. Pymol: An open-source molecular graphics tool. CCP4 Newsletter on protein crystallography. 2002;40:82-92.
16 Chen CC, Hwang JK, Yang JM. (PS)2-v2: template-based protein structure prediction server. BMC Bioinformatics. 2009;10:366. doi: 10.1186/1471-2105-10-366. PubMed PMID: 19878598; PubMed Central PMCID: PMCPMC2775752.
17 Wu S, Zhang Y. LOMETS: a local meta-threading-server for protein structure prediction. Nucleic Acids Res. 2007;35:3375-82. doi: 10.1093/nar/gkm251. PubMed PMID: 17478507; PubMed Central PMCID: PMCPMC1904280.
18 Simossis V, Heringa J. Optimally segmented consensus secondary structure prediction. Bioinformatics. 2004.
19 McGuffin LJ, Bryson K, Jones DT. The PSIPRED protein structure prediction server. Bioinformatics. 2000;16:404-5. doi: 10.1093/bioinformatics/16.4.404. PubMed PMID: 10869041.
20 Geourjon C, Deleage G. SOPMA: significant improvements in protein secondary structure prediction by consensus prediction from multiple alignments. Comput Appl Biosci. 1995;11:681-4. doi: 10.1093/bioinformatics/11.6.681. PubMed PMID: 8808585.
21 Vriend G. WHAT IF: a molecular modeling and drug design program. J Mol Graph. 1990;8:52-6, 29. doi: 10.1016/0263-7855(90)80070-v. PubMed PMID: 2268628.
22 Tina KG, Bhadra R, Srinivasan N. PIC: Protein Interactions Calculator. Nucleic Acids Res. 2007;35:W473-6. doi: 10.1093/nar/gkm423. PubMed PMID: 17584791; PubMed Central PMCID: PMCPMC1933215.
23 Morris GM, Huey R, Lindstrom W, Sanner MF, Belew RK, Goodsell DS, et al. AutoDock4 and AutoDockTools4: Automated docking with selective receptor flexibility. J Comput Chem. 2009;30:2785-91. doi: 10.1002/jcc.21256. PubMed PMID: 19399780; PubMed Central PMCID: PMCPMC2760638.
24 Mills N. ChemDraw Ultra 10.0 CambridgeSoft, 100 CambridgePark Drive, Cambridge, MA 02140. www.cambridgesoft.com. Commercial Price: $1910 for download, $2150 for CD-ROM; Academic Price: $710 for download, $800 for CD-ROM. Journal of the American Chemical Society. 2006;128:13649-50. doi: 10.1021/ja0697875.
25 Zakariazadeh M, Barzegar A, Soltani S, Aryapour H. Developing 2D-QSAR models for naphthyridine derivatives against HIV-1 integrase activity. Medicinal Chemistry Research. 2015;24:2485-504. doi: 10.1007/s00044-014-1305-5.
26 Karami K, Rafiee M, Lighvan ZM, Zakariazadeh M, Faal AY, Esmaeili S-A, et al. Synthesis, spectroscopic characterization and in vitro cytotoxicities of new organometallic palladium complexes with biologically active β-diketones; Biological evaluation probing of the interaction mechanism with DNA/Protein and molecular docking. Journal of Molecular Structure. 2018;1154:480-95. doi: 10.1016/j.molstruc.2017.10.059.
27 Gunsteren Wv, Billeter S, Eising A, Hünenberger P, Krüger P, Mark A, et al. Biomolecular simulation: the GROMOS96 manual and user guide. Verlag der Fachvereine Hochschulverlag AG an der ETH Zurich. 1996.
28 van Aalten DM, Bywater R, Findlay JB, Hendlich M, Hooft RW, Vriend G. PRODRG, a program for generating molecular topologies and unique molecular descriptors from coordinates of small molecules. J Comput Aided Mol Des. 1996;10:255-62. doi: 10.1007/BF00355047. PubMed PMID: 8808741.
29 Andarzi Gargari S, Barzegar A, Tarinejad A. The role of phenolic OH groups of flavonoid compounds with H-bond formation ability to suppress amyloid mature fibrils by destabilizing beta-sheet conformation of monomeric Abeta17-42. PLoS One. 2018;13:e0199541. doi: 10.1371/journal.pone.0199541. PubMed PMID: 29953467; PubMed Central PMCID: PMCPMC6023135.
30 Pettersen EF, Goddard TD, Huang CC,

Couch GS, Greenblatt DM, Meng EC, et al. UCSF Chimera--a visualization system for exploratory research and analysis. J Comput Chem. 2004;25:1605-12. doi: 10.1002/jcc.20084. PubMed PMID: 15264254.

31 Humphrey W, Dalke A, Schulten K. VMD: visual molecular dynamics. J Mol Graph. 1996;14:33-8, 27-8. doi: 10.1016/0263-7855(96)00018-5. PubMed PMID: 8744570.

32 Hess B. P-LINCS: A Parallel Linear Constraint Solver for Molecular Simulation. J Chem Theory Comput. 2008;4:116-22. doi: 10.1021/ct700200b. PubMed PMID: 26619985.

33 Schuttelkopf AW, van Aalten DM. PRODRG: a tool for high-throughput crystallography of protein-ligand complexes. Acta Crystallogr D Biol Crystallogr. 2004;60:1355-63. doi: 10.1107/S0907444904011679. PubMed PMID: 15272157.

34 Kumar CV, Swetha RG, Anbarasu A, Ramaiah S. Computational Analysis Reveals the Association of Threonine 118 Methionine Mutation in PMP22 Resulting in CMT-1A. Adv Bioinformatics. 2014;2014:502618. doi: 10.1155/2014/502618. PubMed PMID: 25400662; PubMed Central PMCID: PMCPMC4220619.

35 Kumar A, Purohit R. Computational screening and molecular dynamics simulation of disease associated nsSNPs in CENP-E. Mutat Res. 2012;738-739:28-37. doi: 10.1016/j.mrfmmm.2012.08.005. PubMed PMID: 22974711.

36 Khabiri M, Freddolino PL. Expression of Concern for "Deficiencies in Molecular Dynamics Simulation-Based Prediction of Protein-DNA Binding Free Energy Landscapes". J Phys Chem B. 2020;124:1115-23. doi: 10.1021/acs.jpcb.8b04187. PubMed PMID: 29741907.

37 Jeffery CJ, Gloss LM, Petsko GA, Ringe D. The role of residues outside the active site: structural basis for function of C191 mutants of Escherichia coli aspartate aminotransferase. Protein Eng. 2000;13:105-12. doi: 10.1093/protein/13.2.105. PubMed PMID: 10708649.

38 Jean-Quartier C, Jeanquartier F, Jurisica I, Holzinger A. In silico cancer research towards 3R. BMC Cancer. 2018;18:408. doi: 10.1186/s12885-018-4302-0. PubMed PMID: 29649981; PubMed Central PMCID: PMCPMC5897933.

39 Ekins S, Mestres J, Testa B. In silico pharmacology for drug discovery: applications to targets and beyond. Br J Pharmacol. 2007;152:21-37. doi: 10.1038/sj.bjp.0707306. PubMed PMID: 17549046; PubMed Central PMCID: PMCPMC1978280.

40 Valerio LG, Jr. Application of advanced in silico methods for predictive modeling and information integration. Expert Opin Drug Metab Toxicol. 2012;8:395-8. doi: 10.1517/17425255.2012.664636. PubMed PMID: 22432718.